Impedance of Bucket Foundations

Torsional, Horizontal and Rocking Motion

Andersen, Lars; Ibsen, Lars Bo; Liingaard, Morten

Published in:
Proceedings of the Sixth International Conference on Engineering Computational Technology

Publication date:
2008

Document Version
Publisher's PDF, also known as Version of record

Paper 189

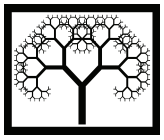

Proceedings of the Sixth International Conference
on Engineering Computational Technology,
M. Papadrakakis and B.H.V. Topping, (Editors),
Civil-Comp Press, Stirlingshire, Scotland

Impedance of Bucket Foundations: Torsional, Horizontal and Rocking Motion

L. Andersen[1], L.B. Ibsen[1] and M.A. Liingaard[2]
[1]Department of Civil Engineering, Aalborg University, Denmark
[2]DONG Energy A/S, Fredericia, Denmark

Abstract

Modern offshore wind turbines are flexible structures with natural frequencies near the excitation frequencies related to wave and wind-induced loads. In order to obtain a reliable prediction of the structural response, the dynamic stiffness of the foundation must be evaluated accurately. This paper concerns the analysis of bucket foundations with focus on torsional motion and coupled horizontal sliding and rocking. The frequency-dependent stiffness is found by means of a three-dimensional coupled boundary-element/finite-element scheme. Comparisons are made with known analytical and numerical solutions, finding that the present boundary-element–finite-element model provides accurate results. The influence of the soil properties as well as the skirt length of the foundation is analysed, and each dynamic stiffness component is computed as function of a non-dimensional frequency.

Keywords: soil–structure interaction, finite elements, boundary elements, dynamics.

1 Introduction

Modern wind turbines are constantly increasing in size. Currently (2008), turbines with rotor diameters and tower heights of more than 100 metres are in production, and the natural frequencies of these structures are close to 0.2 Hz. This may be critical regarding the excitation by wave and wind-induced loads. In particular, the rotor blades pass the tower at a frequency which is very close to the first natural frequency. Hence, to predict the dynamic response and the fatigue lifespan of a wind turbine, the dynamic stiffness of the structure must be modelled with sufficiently high accuracy. This includes an adequate model of the soil–structure interaction.

Depending on the seabed and subsoil at a given site, offshore wind turbines are typically placed on monopiles or gravitational foundations. Recently, the bucket foundation has been developed as a hybrid between these two foundation concepts. Based on the same principles as the suction anchors widely applied in the offshore oil and gas industry, the bucket foundation is designed to withstand torsional and rocking moments as well as horizontal forces in addition to vertical loads.

The purpose of this paper is to evaluate the dynamic stiffness, or impedance, of bucket foundations with emphasis on torsional vibrations and coupled horizontal sliding and rocking. The torsional vibrations of rigid massless footings resting on a homogeneous elastic half-space were studied by Luco and Westman [1] who solved the system as a mixed boundary-value problem with prescribed conditions under the foundation and zero traction at the remaining free surface. The effects of material damping on torsional vibrations were reported by Veletsos and Damodaran Nair [2], whereas Wong and Luco [3] presented tables with horizontal, coupling, rocking, vertical and torsional impedances for rigid massless square foundations resting on layered viscoelastic soil. A generalisation to footings with an arbitrary shape was provided by Andersen and Clausen [4].

Mita and Luco [5] evaluated the impedance functions for rigid square foundations embedded in a homogeneous elastic half-space by means of a hybrid approach, whereas Emperador and Domínguez [6] applied the boundary-element (BE) method for analysis of the dynamic response of axisymmetric embedded foundations. Approximate closed-form solutions for the torsional impedance of circular embedded foundations were reported by Novak and Sachs [7] as well as Avilés and Pérez-Rocha [8]. The coupled horizontal sliding and rocking motion of surface footings were examined by, for example, Veletsos and Wei [9]. This work will be used as reference solution for the subsequent analyses of the coupled horizontal–moment vibrations of the bucket foundation. An extensive review of the work on coupled horizontal–moment vibrations of foundations was presented by Bu and Lin [10].

In the next section, the static and dynamic stiffness of the bucket foundation are defined and a presentation of the coupled boundary-element/finite-element (BE/FE) scheme applied for the numerical analysis is given. The torsional dynamic stiffness of the bucket foundation is presented in Section 3 and the results for the coupled horizontal sliding and rocking motion are given in Section 4. The main conclusions are given in Section 5.

2 Computational model

2.1 Coupled boundary-element/finite-element model

Wave propagation in the subsoil is modelled by the boundary-element (BE) method. A homogeneous viscoelastic domain with the boundary Γ is considered in two and three dimensions. In the first case, plane strain is assumed and in either situation the

complex amplitudes of the displacements and tractions, $U_i(\mathbf{x},\omega)$ and $P_i(\mathbf{x},\omega)$, on the boundary Γ are related by the integral identity [11]

$$C(\mathbf{x})\,U_i(\mathbf{x},\omega) + \int_\Gamma P^*_{ik}(\mathbf{x},\omega;\mathbf{y})U_k(\mathbf{y},\omega)d\Gamma_\mathbf{y} = \int_\Gamma U^*_{ik}(\mathbf{x},\omega;\mathbf{y})P_k(\mathbf{y},\omega)d\Gamma_\mathbf{y}. \quad (1)$$

It has been assumed that no forces are applied in the interior of domain. The tensors $U^*_{ik}(\mathbf{x},\omega;\mathbf{y})$ and $P^*_{ik}(\mathbf{x},\omega;\mathbf{y})$ denote the components of the Green's function tensors for the displacement and surface traction, respectively. These describe the response at point $\mathbf{x}$ in direction i to a unit-amplitude point force or displacement applied at point $\mathbf{y}$ in direction k and varying harmonically at the circular frequency ω. The scalar quantity $C(\mathbf{x})$ only depends on the geometry of the boundary at point $\mathbf{x}$.

The boundary-integral equation (1) is evaluated by discretization of the physical fields into nodal values and interpolation by local quadratic shape functions $\Phi_j(\mathbf{x})$ over space,

$$\mathbf{U}(\mathbf{x},\omega) = \Phi_j(\mathbf{x})\mathbf{U}_j(\omega), \quad \mathbf{P}(\mathbf{x},\omega) = \Phi_j(\mathbf{x})\mathbf{P}_j(\omega), \quad (2)$$

where $\mathbf{U}_j(\omega)$ and $\mathbf{P}_j(\omega)$ denote the vectors storing the amplitudes of the displacements and tractions, respectively, at the nodes of boundary element j. Insertion of Equation (2) into Equation (1) provides the system of equations for a BE domain,

$$\mathbf{H}(\omega)\,\mathbf{U}(\omega) \;=\; \mathbf{G}(\omega)\,\mathbf{P}(\omega), \quad (3)$$

where the geometry constants $C(\mathbf{x})$ are absorbed into the diagonal of $\mathbf{H}(\omega)$. The vectors $\mathbf{U}(\omega)$ and $\mathbf{P}(\omega)$ store the displacements and tractions, respectively, for all nodes on Γ, whereas $\mathbf{H}(\omega)$ and $\mathbf{G}(\omega)$ store the influence from degree-of-freedom k to degree-of-freedom i for the displacement and traction, respectively. Due to the singularities of the Green's functions, special attention has to be made with regard to the contributions from a node to itself. In the present analysis, the weak singularities of $U^*_{ik}(\mathbf{x},\omega;\mathbf{y})$ are treated by a coordinate transformation [11], whereas the the diagonal terms of $\mathbf{H}(\omega)$ are evaluated by a local enclosing-elements technique [12, 13].

The bucket foundation is modelled by continuum finite elements, again employing quadratic interpolation. For the finite-element (FE) part of the model, the system of equations may be expressed in the well-known form

$$\left(-\mathbf{M}\omega^2 + \mathrm{i}\mathbf{C} + \mathbf{K}\right)\mathbf{U} = \mathbf{K}_{FE}\mathbf{U} = \mathbf{F}, \quad (4)$$

where $\mathbf{M}$, $\mathbf{C}$ and $\mathbf{K}$ are the mass, damping and stiffness matrices, respectively, whereas $\mathbf{U}$ and $\mathbf{F}$ are the nodal displacements and forces, respectively. Finally, $\mathrm{i} = \sqrt{-1}$ is the imaginary unit. Hysteretic material dissipation is assumed, i.e. $\mathbf{C} = \eta\mathbf{K}$. Hence, the damping term is independent of the circular frequency, ω.

A coupling of the FE and the BE regions is carried out in a context of nodal forces, i.e. in a finite element manner. This involves that each boundary element domain be transformed into a *macro finite element* as depicted in Figure 1. Here $\mathbf{T}$ is a frequency independent transformation matrix expressing the relationship between the nodal forces and the surface traction applied over the surface of the BE domain. The

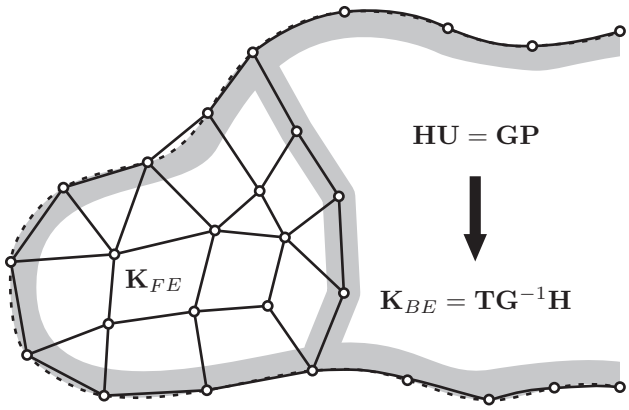

Figure 1: Coupling of finite elements with a boundary element domain.

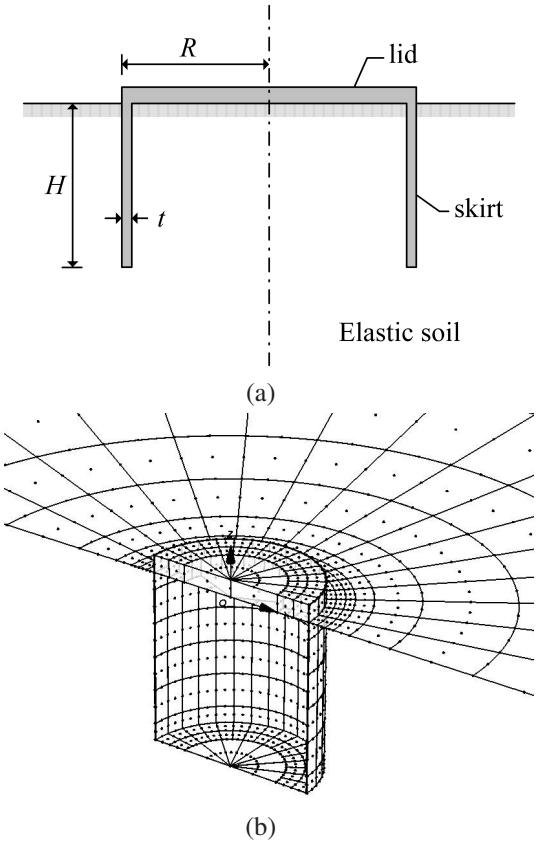

Figure 2: Bucket foundation: (a) geometry and (b) BE/FE model.

resulting coupled BE/FE scheme has been implemented in the computer code TEA [12] for plane-strain analysis and BEASTS [13] for three-dimensional analysis.

The BE/FE model of the foundation consists of four sections: a massless finite-element section that forms the top of the foundation where the load is applied, a finite-element section of the skirts, a boundary-element domain inside the skirts and, finally, a boundary-element domain outside the skirts that also forms the free surface. In to-

tal, approximately 100 finite elements and 350 boundary elements are employed. The mesh of the free surface is truncated at a distance of six times the radius R away from the centre of the foundation. The connection between soil and foundation corresponds to the condition of 'rough' contact, since the foundation and the surrounding soil have common degrees of freedom. The three-dimensional model is illustrated in Figure 2b. Due to geometrical symmetry, only half the foundation is included. In the case of torsional vibrations, the applied load as well as the displacement response is anti-symmetric, whereas symmetric loads and displacements occur in the case of horizontal sliding and rocking.

2.2 Static and dynamic stiffness formulation

The lid of the bucket foundation is relatively stiff compared to the skirts and the subsoil. Hence, it may be simplified to a rigid foundation with six degrees of freedom: one vertical, two horizontal, two rocking and one torsional. The six degrees of freedom and the corresponding forces and moments are shown in Figure 3. For a harmonic excitation with the cyclic frequency ω, the vector of forces and moments $\mathbf{R}$ is equal to the dynamic stiffness matrix $\mathbf{K}$ times the vector of displacements and rotations $\mathbf{U}$, i.e. $\mathbf{R} = \mathbf{KU}$. The component form can be written as

$$\begin{bmatrix} V/G_sR^2 \\ H_1/G_sR^2 \\ H_2/G_sR^2 \\ T/G_sR^3 \\ M_1/G_sR^3 \\ M_2/G_sR^3 \end{bmatrix} = \begin{bmatrix} K^*_{VV} & 0 & 0 & 0 & 0 & 0 \\ 0 & K^*_{HH} & 0 & 0 & 0 & -K^*_{HM} \\ 0 & 0 & K^*_{HH} & 0 & K^*_{HM} & 0 \\ 0 & 0 & 0 & K^*_{TT} & 0 & 0 \\ 0 & 0 & K^*_{MH} & 0 & K^*_{MM} & 0 \\ 0 & -K^*_{MH} & 0 & 0 & 0 & K^*_{MM} \end{bmatrix} \begin{bmatrix} W/R \\ U_1/R \\ U_2/R \\ \theta_T \\ \theta_{M1} \\ \theta_{M2} \end{bmatrix}, \quad (5)$$

where G_s is the shear modulus of the soil. The coupling terms, K^*_{HM} and K^*_{MH}, are assumed to be equal, since a symmetric stiffness matrix is expected. This assumption is investigated later.

The components in $\mathbf{K}$ are functions of the cyclic frequency ω and Poisson's ratio of the soil ν_s, and $\mathbf{K}$ reflects the dynamic stiffness of a rigid massless foundation. The

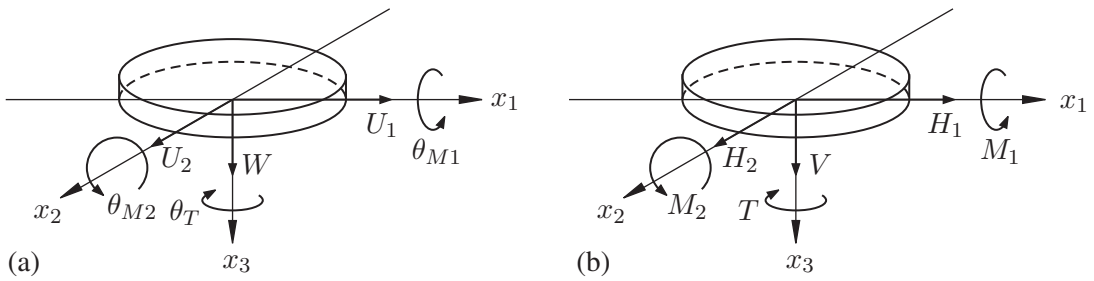

Figure 3: Degrees of freedom for a rigid surface footing: (a) displacements and rotations, and (b) forces and moments.

components of $\mathbf{K}$ can be written as

$$K_{ij}^{*}(a_0) = K_{ij}^{0}\left[k_{ij}\left(a_0\right) + \mathrm{i}a_0 c_{ij}\left(a_0\right)\right], \qquad (i,j = H,M,T,V), \tag{6}$$

where K_{ij}^{0} is the static value of stiffness component ij, k_{ij} and c_{ij} are the dynamic stiffness and damping coefficients, respectively, and $\mathrm{i} = \sqrt{-1}$ is the imaginary unit. Furthermore, $a_0 = \omega R/c_S$ is the dimensionless frequency where $c_S = \sqrt{G_s/\rho_s}$ is the shear-wave velocity of the soil. The mass density of the soil is ρ_s. The real part of $K_{ij}^{*}(a_0)$ is related to the stiffness and inertia properties of the soil–structure system, whereas the imaginary part describes the damping of the system. For a soil without material dissipation, c_{ij} reflects the geometric damping, i.e. the radiation of waves into the subsoil. However, in the present analyses hysteretic material damping with the loss factor η_s is introduced, represented by a complex shear modulus, $G_s^{*} = G_s(1 + \mathrm{i}\eta_s)$.

The information provided by the real and imaginary parts of Equation (6) tends to be inconclusive in some situations, and for that reason it is convenient to examine the magnitude and phase angle of Equation (6). The magnitude $|K_{ij}^{*}|$ and the phase angle ϕ_{ij} of K_{ij}^{*} are given by

$$|K_{ij}^{*}| = |K_{ij}^{0}|\sqrt{\left(k_{ij}\right)^2 + \left(a_0 c_{ij}\right)^2}, \qquad \phi_{ij} = \operatorname{atan}\left(\frac{a_0 c_{ij}}{k_{ij}}\right). \tag{7}$$

The magnitude and phase-angle representation of the dynamic stiffness will be used throughout the paper.

3 Stiffness for torsional vibrations

In this section, the torsional stiffness of the foundation is investigated. Poisson's ratio has no impact on the torsional stiffness, since torsional vibrations of the bucket foundation only produce shear waves. Hence, the analysis only concerns the variation of the normalised torsional stiffness due to a change in the skirt length H, cf. Figure 2a. The section consists of three parts. Firstly, the static torsional stiffness obtained by the BE/FE model is presented and compared with results from a static finite-element analysis performed in ABAQUS [14]. In the second part, the dynamic stiffness for torsional vibrations is examined. The third subsection presents the limiting damping parameter for the high-frequency behaviour.

3.1 Static stiffness

The static torsional stiffness K_{TT}^{0} corresponds to the stiffness of the soil–foundation system without any inertial or material dissipation effects. The BE/FE model cannot provide the static stiffness, since a positive value of the excitation frequency is required in the program BEASTS [13]. Instead, an estimate is achieved by analysing the response at a very low frequency, $a_0 = 0.01$, where the inertial effects are negligible. To check the BE/FE solution, a static finite-element solution has been computed by

H/D	K^0_{TT} (FE)	K^0_{TT} (BE/FE)	Deviation (%)
1/4	12.94	13.15	-1.63
1	32.36	32.43	-0.23
2	56.88	53.90	$+5.52$

Table 1: Static torsional stiffness for different skirt lengths

means of a three-dimensional ABAQUS model. The finite-element model consists of the bucket foundation and a near-field soil domain modelled by finite elements with quadratic interpolation and a far-field soil domain modelled by infinite elements. The ABAQUS model contains approximately 200,000 degrees of freedom.

In the present analysis, the soil properties are $G_s = 1$ MPa and $\nu_s = 1/3$, whereas the foundation has a Young's modulus of $E_f = 210$ GPa and a Poisson's ratio of $\nu_f = 0.25$ corresponding to construction steel. Here, the material properties of the soil and the foundation are identified by the subscripts s and f, respectively. The foundation has the skirt thickness $t = 50$ mm and the radius $R = 5$ m corresponding to the diameter $D = 2R = 10$ m. Finally, a relatively high thickness and stiffness ensures that the lid behaves almost as a rigid body.

In Table 1, K^0_{TT} is given for three normalised skirt lengths defined by $H/D = 1/4$, 1 and 2, respectively. It is observed that the two numerical models provide similar results, indicating that the ABAQUS and BEASTS models are nearly converged. The deviation is partly due to the fact that better convergence has been obtained by the FE solution, however at the cost of significantly more degrees of freedom and, as a result of this, long computation times. Further, as already mentioned the static BE/FE solution is actually an estimate obtained with $a_0 = 0.01$.

3.2 Dynamic stiffness

The normalised torsional dynamic stiffness, $|S_{TT}|/K^0_{TT}$ is analysed for three normalised skirt lengths, $H/D = 1/4$, 1 and 2, and in the normalised frequency range $a_0 \in$]0;10]. A comparison is made with two reference solutions. Firstly, the normalised torsional dynamic stiffness has been found for a surface footing. This result has been obtained by means of a three-dimensional BE/FE model with no skirt, i.e. with $H = 0$. Secondly, the dynamic stiffness per unit length of an infinite hollow cylinder subjected to dynamic excitation is evaluated by means of the two-dimensional coupled BE/FE program TEA [12]. The hollow cylinder is modelled with 64 quadrilateral finite elements employing quadratic interpolation. The interior and exterior soil domains are modelled with 64 boundary elements each. The model is sketched in Figure 4, and plane strain is assumed.

In all the analyses, the soil has the shear modulus $G_s = 1$ MPa, a Poisson's ratio of $\nu_s = 1/3$, the mass density $\rho_s = 1000$ kg/m^3 and the loss factor $\eta_s = 5\%$. The foundation has a Young's modulus of $E_f = 210$ GPa, a Poisson's ratio of $\nu_f = 0.25$, the loss factor $\eta_f = 2\%$ and the skirt thickness $t = 50$ mm. In order to model a

massless foundation, the mass density is $\rho_f = 0$ for the lid of the caisson and $\rho_f = \rho_s$ for the skirt. In any case, the inertia of the skirt is insignificant compared with the contribution from the skirt to the stiffness of the bucket foundation.

As indicated by Figure 5, the normalised magnitudes of the torsional impedance are similar for the surface footing, the caissons and the infinite cylinder in the frequency interval $a_0 \in [0; 2]$. Note that the actual magnitude of the impedance for each skirt length is scaled by the static stiffness values given in Table 1. For $a_0 > 2$ the impedance of all the skirted foundations are greater than the impedance of the surface footing. The dynamic stiffness of the caisson with a relatively small embedment depth ($H/D = 1/4$) varies smoothly with the frequency. However, the normalised magnitudes for $H/D = 1$ and 2 are characterised by distinct peaks close to $a_0 = 4$, 7 and 10. The peaks become more pronounced when the skirt length is increased, and the behaviour corresponds well to that of the infinite cylinder. Between the peaks, the normalised torsional impedances for all skirt lengths are nearly identical in magnitude. This is even the case for the infinite cylinder. However, K^0_{TT} (and therefore also $|S_{TT}|$) is increased significantly with an increase in the skirt length, cf. Table 1.

The local peaks in the normalised magnitude are associated with a significant change in the phase angle, ϕ_{TT}. The fact that the oscillations are repeated for equal distances in frequency implies that the frequencies at the local peaks correspond to antiresonance modes of the soil inside the suction caisson.

3.3 High-frequency limit

The limiting damping parameter C^∞_{TT} of the bucket foundation consists of two contributions: one from the vibration of the lid and one originating from the vibration of the

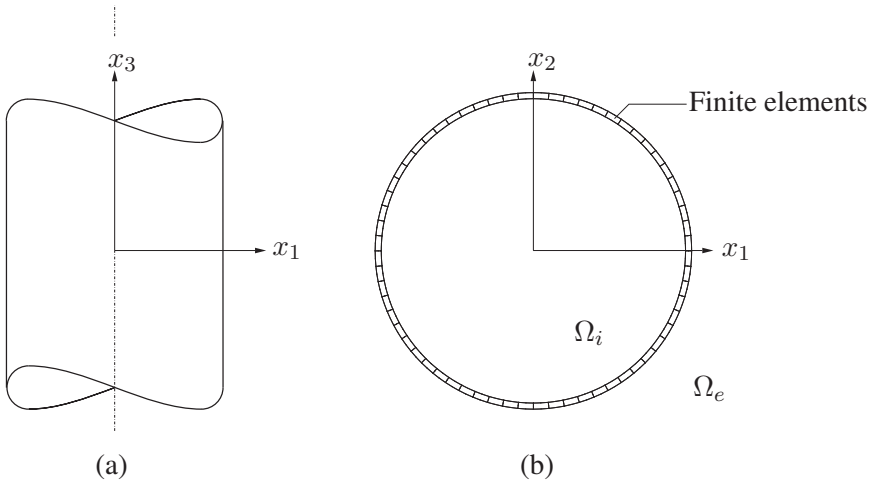

Figure 4: Infinite hollow cylinder (a) and two-dimensional BE/FE model (b). The interior and exterior boundary-element domains are denoted Ω_i and Ω_e, respectively.

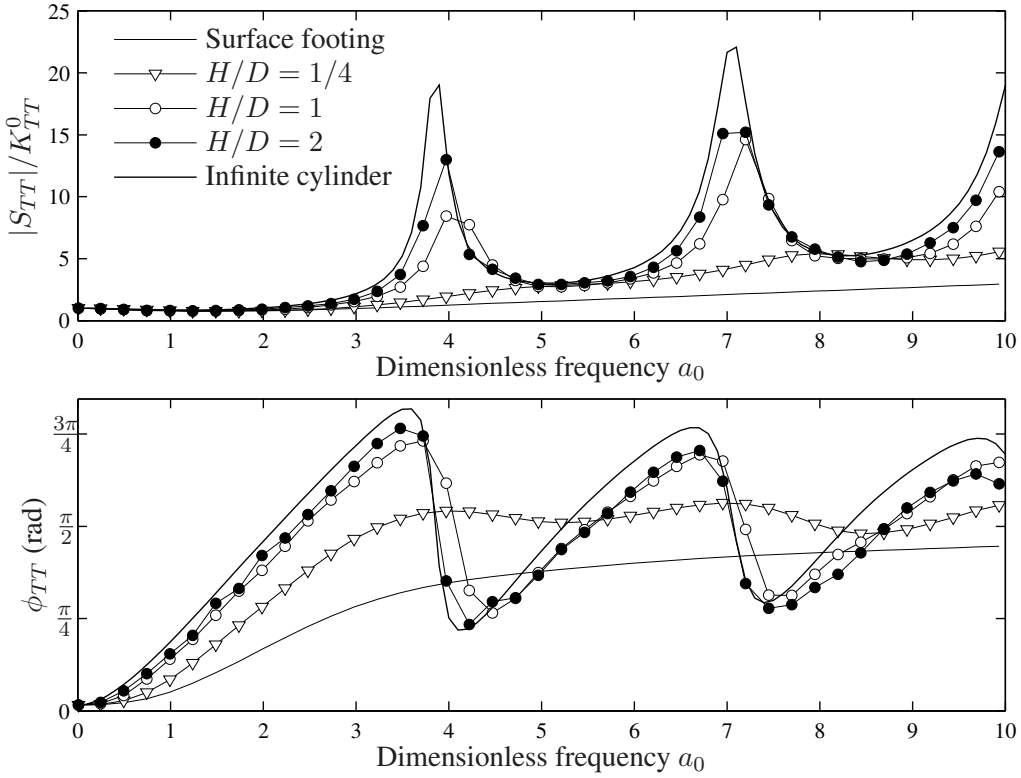

Figure 5: Torsional impedance at different skirt lengths.

skirt. Thus, C^{∞}_{TT} of the bucket foundation is given by

$$C^{\infty}_{TT} = \rho_s c_S J_{lid} + (2\rho_s c_S A_{skirt})\, R^2, \tag{8}$$

where J_{lid} is the polar moment of inertia of the lid about the axis of rotation and A_{skirt} is the surface area of skirt. Note that S-waves are generated both inside and outside the skirt; hence, the factor '2' in the latter contribution in Equation (8). The radius R is the distance from skirt to the axis of rotation.

4 Stiffness for coupled sliding and rocking

In this section, the coupled sliding–rocking vibrations are investigated for several different combinations of the mechanical properties of the soil–foundation system. The first case concerns the effects of Poisson's ratio on the stiffness. The second analysis investigates the variation of the stiffness due to a change in the skirt length. Finally, the limiting damping parameters for vibration in the high-frequency range are given.

4.1 Boundary-element/finite-element model

The geometry and the discretization in the BE/FE models employed for the present analyses are as described in the previous section. However, the load is applied differently. For a given excitation frequency, two analyses are performed: one analysis with horizontal loading at the base of the lid of the caisson, and one analysis with a set of opposing vertical forces that are applied at either side of the foundation in order to create a rocking moment. The first analysis provides a relation between the horizontal force and the resulting displacements and rotations. The second analysis relates the applied moment to the resulting displacements and rotations. The system can be written as a subset of Equation (5), given as

$$\begin{bmatrix} H_1/G_sR^2 \\ M_2/G_sR^3 \end{bmatrix} = \begin{bmatrix} S_{HH} & -S_{HM} \\ -S_{MH} & S_{MM} \end{bmatrix} \begin{bmatrix} U_1/R \\ \theta_{M2} \end{bmatrix}. \tag{9}$$

These two equations are solved simultaneously in order obtain the complex horizontal-sliding impedance, S_{HH}, the rocking-moment impedance, S_{MM}, and the coupling impedances, S_{HM} and S_{MH}. As already mentioned and further discussed below, S_{HM} is identical to S_{MH} within the precision of the model.

4.2 Static stiffness

Similarly to the case of torsional vibrations, the static stiffness coefficients of the foundation–soil system have been approximated by applying the BE/FE models at the frequency $a_0 = 0.01$. The BE/FE solutions are compared with the results of static finite element analyses in ABAQUS. The non-dimensional values of K^0_{HH}, K^0_{MM}, K^0_{HM} and K^0_{MH} are given for two cases:

Different skirt lengths: The static stiffness components are given for various ratios between the foundation diameter D and the length of the skirt H in Table 2. The soil properties are $G_s = 1$ MPa and $\nu_s = 1/3$.

Different Poisson's ratios: The variation of static stiffness with respect to Poisson's ratio is shown in Table 2. Here, $H/D = 1$ and $G_s = 1$ MPa.

Note that the values in parentheses in Table 2 are obtained by the static finite-element analyses in ABAQUS, serving as the reference solution. The data are shown for fixed material properties of the foundation ($E_f = 210$ GPa, $\nu_f = 0.25$). The foundation radius is $R = 5$ m and the skirt thickness is $t = 50$ mm. In addition to the analyses listed above, it may be relevant to check the influence of the skirt flexibility. However, a preliminary study indicates that changes in E_f and t within the range that is relevant for bucket foundations have little impact on the overall performance of the foundation compared with the skirt length and the Poisson's ratio of the ground. Therefore, this study will not be included in the present analysis.

The largest deviation between the results from the BE/FE model and the ABAQUS models in Table 2 are 7.4%, 7.2% and 16.8% for the sliding, rocking and coupling term, respectively. Furthermore, the assumption of $K^0_{HM} = K^0_{MH}$ holds true. The maximum deviation between K^0_{HM} and K^0_{MH} is 11% in the BE/FE model and only 3.3% for the ABAQUS model. In general there is a good agreement between the values of the impedance components computed by the FE and the BE/FE models. As expected, all the stiffness components increase with the skirt length, cf. Table 2. The magnitude of the sliding, rocking and coupling terms increase slightly with Poisson's ratio, ν_s. This is due to the fact that an increase in ν_s for a fixed value of G_s implies an increase in the Young's modulus, $E_s = 2G_s(1 + \nu_s)$.

4.3 Dynamic stiffness—variation of Poisson's ratio

The dynamic stiffness for different Poisson's ratios is presented in this section. The skirt length is fixed (H/D = 1), and the remaining model properties are: $G_s = 1.0$ MPa, $\rho_s = 1000$ kg/m^3, $\eta_s = 5\%$, $E_f = 210$ GPa, $\nu_f = 0.25$, $\eta_f = 2\%$ and $t = 50$ mm. In order to model a massless foundation $\rho_f = 0$ for the lid of the caisson and $\rho_f = \rho_s$ for the skirt. In Figures 6–8, the results are shown for five different values of Poisson's ratio and for the frequency range $a_0 \in$]0;6]. Note that the range in Poisson's ratio is thought to cover fully drained ($\nu_s = 0.1 - 0.2$) to undrained ($\nu_s = 0.495$) conditions.

The analytical solution for a surface footing proposed by Veletsos and Wei [9] is included as reference. Two numerical models of a massless surface footing are included for comparison with the analytical solution. The sliding and rocking impedance of the surface footing have been determined by a BE/FE model. In the case of the coupling between horizontal sliding and rocking, numerical experiments indicate that convergence of the impedance cannot be established with a reasonably low number of degrees of freedom in the BE/FE model. In particular it has been found that both the magnitude and the phase of the impedance is strongly dependent on the distance from the footing to the truncation edge of the free ground surface. Adaptive meshing could possibly improve the accuracy versus the number of degrees of freedom, but this facility is currently not available in the BE/FE software.

		K^0_{HH}		K^0_{MM}		K^0_{HM}		K^0_{MH}	
$H/D =$	1/4	8.00	(7.47)	8.51	(8.41)	-3.13	(-2.68)	-2.78	(-2.68)
	1	13.92	(12.98)	52.91	(49.73)	-18.28	(-16.11)	-17.20	(-16.12)
	2	18.61	(18.47)	198.87	(193.41)	-44.80	(-43.02)	-43.54	(-43.12)
$\nu_s =$	0.1	12.49	(11.62)	49.75	(46.91)	-17.11	(-15.19)	-16.09	(-15.21)
	0.2	13.01	(12.14)	50.83	(47.92)	-17.50	(-15.53)	-16.47	(-15.55)
	0.333	13.92	(12.98)	52.91	(49.73)	-18.28	(-16.11)	-17.20	(-16.12)
	0.4	14.54	(13.53)	54.42	(51.02)	-18.86	(-16.54)	-17.75	(-16.53)
	0.495	15.74	(14.51)	57.79	(53.98)	-20.19	(-17.42)	-18.95	(-17.39)

Table 2: Static stiffness for coupled sliding and rocking.

Therefore, instead of the coupled BE/FE model based on the Green's function for the full-space, an alternative method proposed by Andersen and Clausen [4] has been applied. Here the solution is established in the wavenumber domain, and the fundamental solution for a half-space is employed. Moreover, the impedance is computed directly by integration of the interaction forces between the footing and the subsoil. This is in contrast to the BE/FE approach, in which the impedance is found by inversion of the dynamic flexibility matrix. The latter approach may involve great inaccuracies with respect to the coupling term since $|S_{HM}|$ is much smaller than $|S_{HH}|$ and $|S_{MM}|$, in particular in the high-frequency range.

The sliding and rocking impedances are clearly dependent on Poisson's ratio. The frequency at the first local extremum in the magnitude of the impedance in Figures 6 and 7 changes significantly with Poisson's ratio. The first peak for $\nu_s = 0.1$ occurs at $a_0 = 3.2$, whereas the first peak for $\nu_s = 0.4$ is placed close to $a_0 = 4.5$. However, the second local extremum is found at the frequency $a_0 = 5.5 - 5.7$ for all values of Poisson's ratio. This behaviour is explained by the fact that sliding and rocking impedances are governed by both shear wave propagation and compression wave propagation. More specifically, the first peak in the response corresponds to antiresonance of P-waves inside the caisson, whereas the second peak corresponds to antiresonance of S-waves. The latter is independent of the Poisson's ratio whereas an increase in ν_s involves an increase in c_P. Hence, the first peak in Figures 6–8 occurs at lower

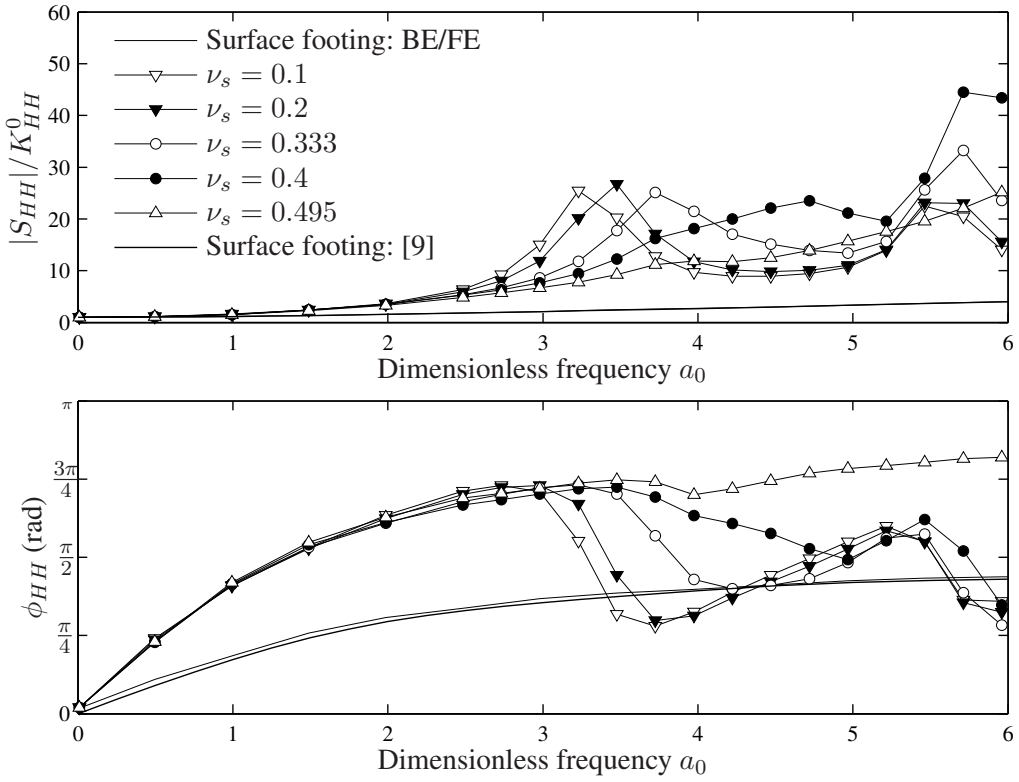

Figure 6: Sliding impedance for different Poisson's ratios.

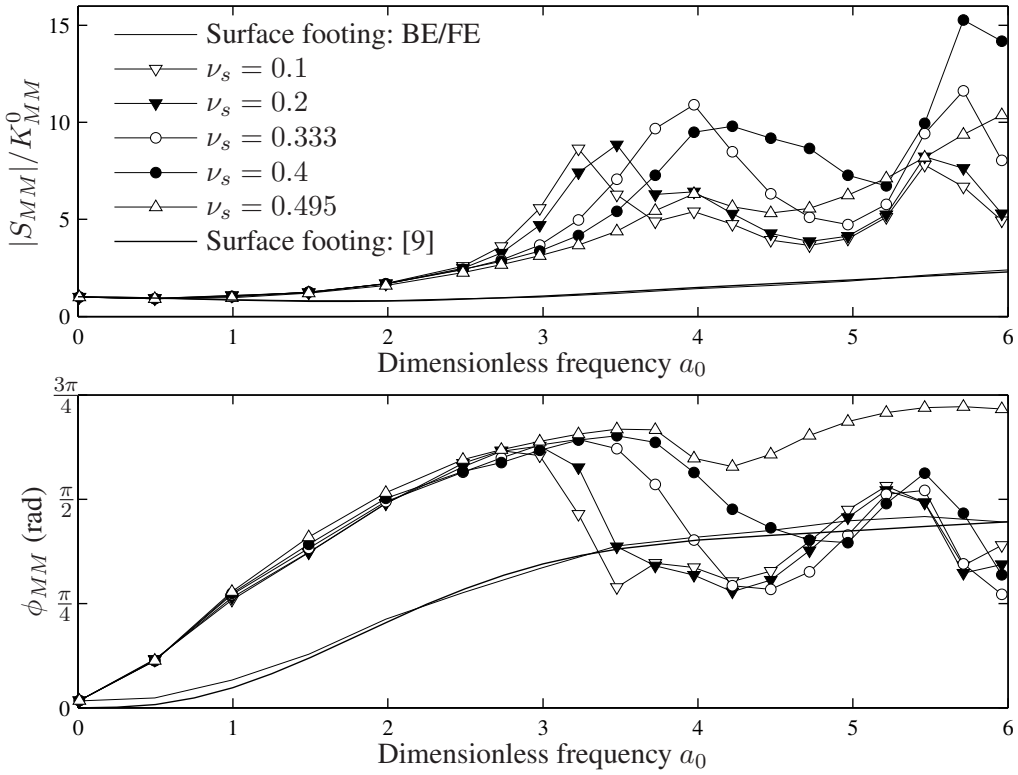

Figure 7: Rocking impedance for different Poisson's ratios.

frequencies for lower Poisson's ratios.

The coupling impedance in Figure 8 follows the pattern of the horizontal sliding and rocking impedances. Hence, an increase in the frequency provides an increase in the magnitude of the coupling impedance over the normalised frequency range $a_0 \in$]0;6]. It is noted that the phase angle of the coupling impedance is close to π radians for $a_0 = 0$ and slightly increasing with the frequency in the range $a_0 \in$]0;6]. Accordingly the static stiffness components K^0_{HM} and K^0_{MH} are negative, see Table 2. It is generally observed that the coupling impedances of the bucket foundation and the surface footing behave differently. Thus, in the case of the surface footing a decrease of both the magnitude and the phase angle of the coupling impedance with frequency is recorded in the interval $a_0 \in$]0;6].

A few remarks on the impedance of the surface footing: The sliding and rocking impedance determined by the BE/FE model agrees very well with the analytical solution reported by Veletsos and Wei [9]. Furthermore, the coupling terms obtained by the alternative method [4] is consistent with the coupling reported by Veletsos and Wei [9]. Note that the analytical solution with respect to the coupling term is an approximation, due to fact that the boundary conditions in the interface between the soil and the footing are partly relaxed. Finally, it is emphasised that the problem of determining the coupling between horizontal sliding and rocking only is encountered for the surface footing. The coupling between horizontal sliding and rocking for the suction caisson is described satisfactorily by the BE/FE model.

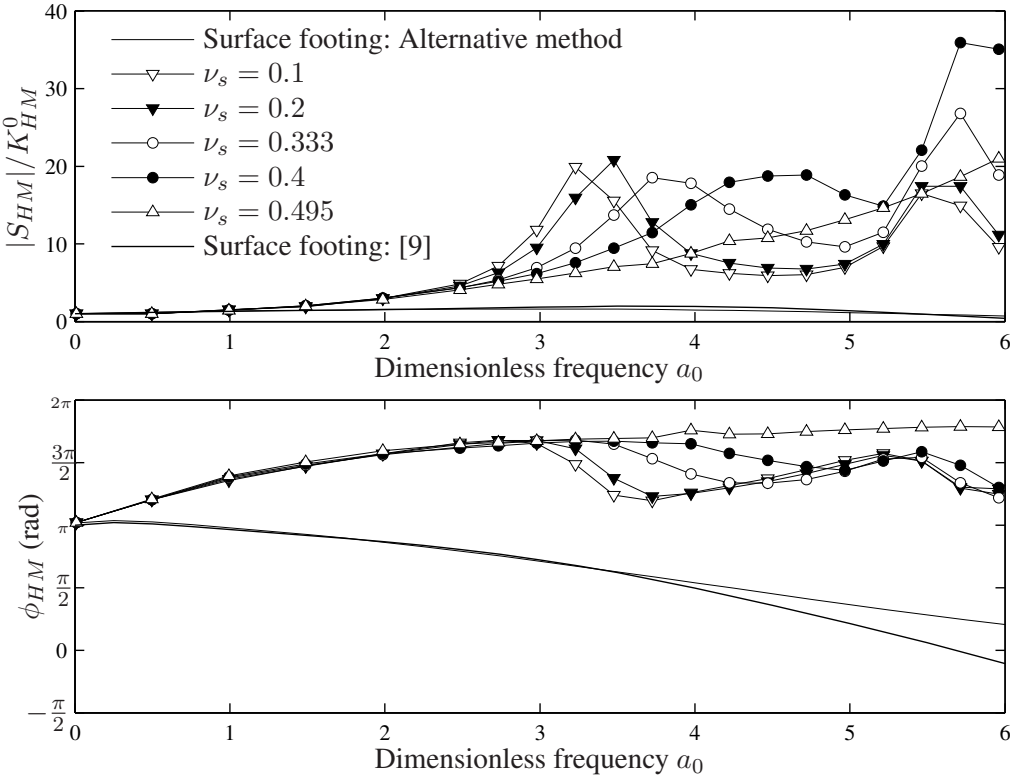

Figure 8: Sliding–rocking coupling impedance for different Poisson's ratios.

4.4 Dynamic stiffness—variation of skirt length

The variation of the coupled dynamic stiffness components with respect to a change in the skirt length H is presented in the following. The model properties are $G_s = 1$ MPa, $\nu_s = 1/3$, $\rho_s = 1000$ kg/m^3, $\eta_s = 5\%$, $E_f = 210$ GPa, $\nu_f = 0.25$, $\eta_f = 2\%$ and $t = 50$ mm. Again, $\rho_f = 0$ for the lid of the caisson and $\rho_f = \rho_s$ for the skirt in order to model a massless foundation.

The magnitudes and the phase angles of the impedance for $H/D = 1/4$, 1 and 2 are shown in Figures 9–11 for the frequency range $a_0 \in$]0;12]. The magnitudes are normalised with respect to the static stiffness coefficients listed in Table 2, and the results achieved with two numerical models of a massless surface footing are included for comparison, see Subsection 4.3. In addition to this, the horizontal sliding impedance of an infinitely long hollow cylinder ($H/D = \infty$) has been computed by application of the two-dimensional BE/FE code TEA as described in Subsection 3.2 for the case of torsional vibrations. Evidently, a similar two-dimensional analysis cannot be performed for the rocking and coupling impedances. With reference to Figure 9, there is no indication of antiresonance of the waves inside the caisson with a relatively small embedment depth (H/D = 1/4), i.e. there are no local peaks in the normalised magnitude of the impedance component for sliding. Thus the dynamic behaviour is similar to that of the surface footing, though the increase of the impedance with increasing

frequency is more pronounced for the skirted foundation than the surface footing.

However, the sliding impedances for $H/D = 1$ and 2 are characterised by a number of local tips and dips. The peaks are not repeated with the normalised frequency interval $\Delta a_0 = \pi$. This is the case for the torsional impedance, where the location of the peaks is governed by the shear waves only. In contrast to this, the location of the peaks for the coupled sliding–rocking impedances are controlled by antiresonance of both shear waves and compression waves. Clearly, the locations of the peaks in the magnitude of the sliding impedance for $H/D = 1$ and 2 correspond to those for the infinitely long cylinder. Likewise, the variation of the phase angle ϕ_{HH} is similar for $H/D = 1$, 2 and ∞, cf. Figure 9. The magnitude of the horizontal impedance (Figure 9) seems to increase with skirt length. However, the change from $H/D = 1/4$ to $H/D = 1$ is significant, whereas only a small change is observed from $H/D = 1$ to $H/D = 2$. The magnitude of the impedance for H/D = 2 is actually below the impedance for $H/D = 1$ at high frequencies. This behaviour suggests that the horizontal vibrations are transmitted to the surrounding soil at relatively shallow depths. Hence, the effects of increasing the skirt length diminish with depth. This is not the case for the moment impedance in Figure 10, where the effects of increasing the skirt length increase with depth. These tendencies are also evident in the static stiffness coefficients listed in Table 2. Finally, the coupling impedance in Figure 11 increases moderately with an increase of the skirt length, and again the phase angle is close to π radians for all frequencies. Otherwise, the overall response is similar to the horizontal

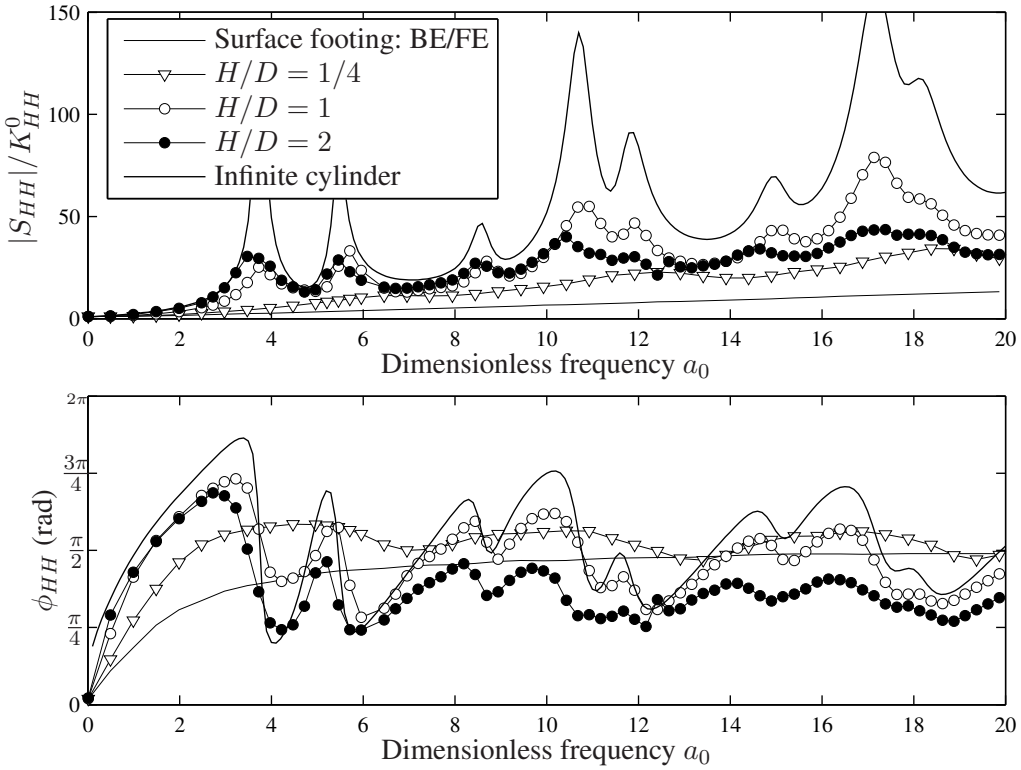

Figure 9: Sliding impedance for different skirt lengths.

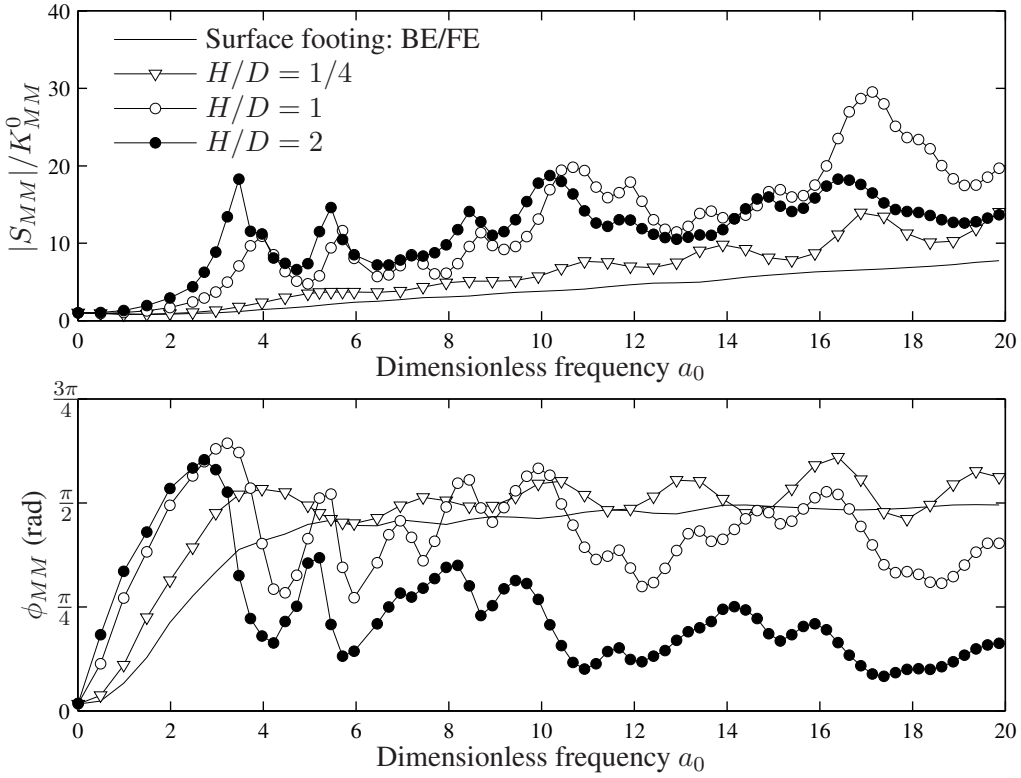

Figure 10: Rocking impedance for different skirt lengths.

and moment impedances.

4.5 High-frequency limit

The total geometrical damping is equal to the sum of the waves radiating from the skirts and the lid of the caisson. The limiting damping parameter for the horizontal vibration (C^{∞}_{HH}) consists of three contributions: shear waves radiating from the lid, shear waves radiating from the skirt parallel to the direction of loading, and compression waves radiating from the skirt perpendicular to the direction of loading. The high-frequency impedance for the rocking and coupling terms consist of similar contributions, see [10, 15, 16, 17, 18] for further details. Assuming that both the lid and the skirts of the bucket foundation are rigid, the limiting damping parameters C^{∞}_{HH}, C^{∞}_{MM} and C^{∞}_{HM} are given by

$$C^{\infty}_{HH} = \rho_s c_S \pi R^2 + 2\rho c_S \pi RH + 2\rho c_P \pi RH, \tag{10a}$$

$$C^{\infty}_{MM} = \rho_s c_P \frac{\pi}{4} R^4 + 2\rho_s c_P \frac{1}{3}\pi RH^3 + 2\rho_s c_S \frac{1}{3}\pi RH^3 + 2\rho_s c_S \pi R^3 H, \tag{10b}$$

$$C^{\infty}_{HM} = -2\rho_s c_S \frac{1}{2}\pi RH^2 - 2\rho_s c_P \frac{1}{2}\pi RH^2 0 = C^{\infty}_{MH}. \tag{10c}$$

Note that waves radiate from both inside and outside the skirts; hence, the factor '2' in front of the appropriate contributions in Equations (10a)–(10c).

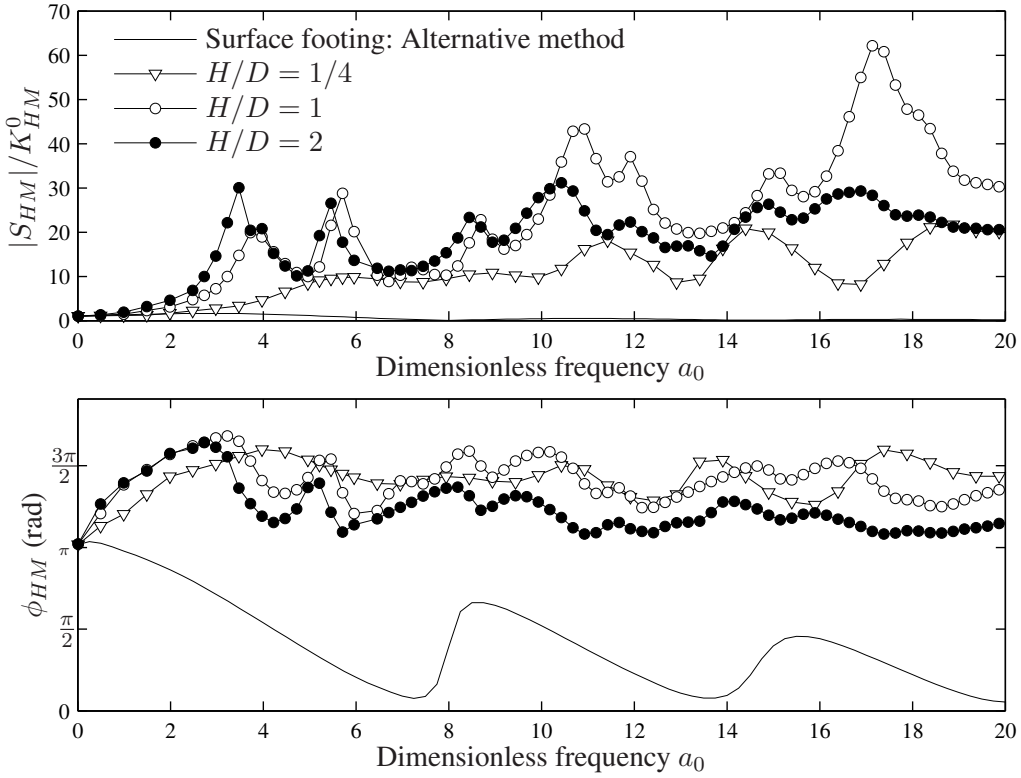

Figure 11: Sliding–rocking coupling impedance for different skirt lengths.

5 Conclusion

The stiffness of bucket foundations with respect to torsional vibrations and coupled sliding–rocking vibrations has been analysed by means of a three-dimensional coupled Boundary-Element/Finite-Element model. The dynamic stiffness components have been found as function of the non-dimensional frequency $a_0 = \omega R/c_S$, where ω is the circular frequency of excitation, R is the radius of the foundation and c_S is the shear-wave velocity of the soil.

All the analyses are carried out for a bucket foundation with a lid diameter of 10 m, a skirt thickness of 50 mm and material properties corresponding to construction steel. It has been found by a preliminary study, not presented in this paper, that slight modifications of the foundation properties has an insignificant impact on the overall results, given that the foundation is in any case much stiffer than the surrounding soil.

5.1 Torsional vibrations

The torsional dynamic stiffness has been analysed with respect to the variation of the stiffness due to a change in the skirt length H. The main conclusions are:

- The static torsional stiffness, K^0_{TT}, obtained with the BE/FE model has been compared with the results from a finite element analysis. There is good agreement between the estimations of K^0_{TT} provided by the two methods with a maximum deviation of 5.52%

- The torsional impedance is independent of Poisson's ratio, since torsional motion of the bucket foundation does not produce compressional waves but only shear waves.

- The magnitude of the static and dynamic torsional stiffness increases with the skirt length.

- The torsional impedance of the suction caisson with a relatively small embedment depth ($H/D = 1/4$) varies smoothly with the frequency, whereas the torsional impedances for $H/D = 1$ and 2 are characterised by distinct peaks in the normalised magnitude close to $a_0 = 4$, 7 and 10.

- The oscillations are repeated for equal distances in frequency, corresponding to antiresonance modes in the soil inside the bucket foundation.

- The torsional impedance of the bucket foundation has been compared with the impedance of an infinite cylinder subjected to a torsional moment. The changes with frequency in the magnitude and the phase angle of the impedance are equivalent for the bucket foundation and the infinite cylinder.

5.2 Coupled sliding and rocking

The impedance related to the coupled sliding–rocking vibrations has been analysed with respect to the effects of changes in Poisson's ratio and the skirt length. The following conclusions can be made:

- The static stiffness has been calculated with a BE/FE model and a finite-element model. The largest deviation of the results of the two models are 7.4%, 7.2% and 16.8% for the sliding, rocking and coupling terms, respectively. Presumably, the finite-element model is slightly better converged than the BE/FE model.

- The two coupling terms between sliding and rocking (and vice versa) are equal, i.e. $K^0_{HM} = K^0_{MH}$, within the accuracy of the analysis. The maximum deviation between K^0_{HM} and K^0_{MH} is 11%

- The sliding and rocking impedances are clearly dependent on Poisson's ratio of the soil, and the local extremum in the magnitude of the impedance changes significantly with Poisson's ratio.

- The effects of increasing the skirt length diminish with depth with respect to the horizontal impedance. The effects of increasing the skirt length enlarge with

depth with respect to the rocking impedance and the sliding–rocking coupling components.

- The coupled sliding–rocking impedances are characterised by a complex wave interference pattern in the soil inside the skirts. The local peaks in the magnitude of the impedance components are not repeated by $\Delta a_0 = \pi$, which is the case for the vertical and torsional impedance components. The location of the peaks for the coupled sliding–rocking impedances are controlled by antiresonance of both shear waves and compression waves.
- The analysis of the horizontal impedance for an infinite hollow cylinder clearly shows the antiresonance frequencies of both shear waves and compression waves for the vibrating cylinder. The results agree well with the horizontal impedance of the suction caissons.

Finally, it is noted that the high-frequency limits of the impedance components have been established for the skirted foundation. These will be applied in combination with the low-frequency impedances obtained with the BE/FE models in future formulations of lumped-parameter models of bucket foundations as described by Andersen and Liingaard [19] for surface footings on layered soil. The lumped-parameter models are to be applied within the aeroelastic codes utilised by the Danish wind-turbine industry for the design of offshore wind turbines.

Acknowledgements

The authors would like to thank the Danish Energy Authority for financial support via the Energy Research Programme "Soil–Structure Interaction of Foundations for Offshore Wind Turbines".

References

[1] J.E. Luco and R.A. Westmann, "Dynamic Response of Circular Footings". Journal of the Engineering Mechanics Division, ASCE, 97, 1381–1395, 1971.

[2] A.S. Veletsos and V.V. Damodaran Nair, "Torsional vibration of viscoelastic foundations", Journal of the Geotechnical Engineering Division, ASCE, 100 (GT3), 225–246, 1974.

[3] H.L. Wong and J.E. Luco, "Tables of impedance functions for square foundations on layered media", Soil Dynamics and Earthquake Engineering, 4 (2), 64–81, 1985.

[4] L. Andersen and J. Clausen, "Impedance of surface footings on layered ground", Computers and Structures, 86, 72–87, 2008.

[5] A. Mita and J.E. Luco, "Impedance functions and input motions for embedded square foundations", Journal of Geotechnical Engineering, ASCE, 115 (4), 491–503, 1989.

[6] J.M. Emperador and J. Domínguez, "Dynamic response of axisymmetric embedded foundations", Earthquake Engineering and Structural Dynamics, 18, 1105–1117, 1989.

[7] M. Novak and K. Sachs, "Torsional and coupled vibrations of embedded footings", Earthquake Engineering and Structural Dynamics, 2, 11–33, 1973.

[8] J. Avilés and L.E. Pérez-Rocha, "A simplified procedure for torsional impedance functions of embedded foundations in a soil layer", Computers and Geotechnics, 19 (2), 97–115, 1996.

[9] A.S. Veletsos and Y.T. Wei, "Lateral and Rocking Vibration of Footings", Journal of the Soil Mechanics and Foundation Engineering Division, ASCE, 97, 1227–1248, 1971

[10] S. Bu and C.H. Lin, "Coupled horizontal-rocking impedance functions for embedded square foundations at high frequency factors", Journal of Earthquake Engineering, 3, 561–587, 1999.

[11] J. Domínguez, "Boundary elements in dynamics", Computational Mechanics Publications, Southampton, 1993.

[12] C.J.C. Jones, D.J. Thompson and M. Petyt, "TEA — A suite of computer programs for elastodynamic analysis using coupled boundary elements and finite elements", ISVR Technical Memorandum 840, Institute of Sound and Vibration Research, University of Southampton, 1999.

[13] L. Andersen and C.J.C. Jones, "BEASTS — a computer program for Boundary Element Analysis of Soil and Three-dimensional Structures", ISVR Technical Memorandum 868, Institute of Sound and Vibration Research, University of Southampton, 2001.

[14] ABAQUS—Version 6.4 2003, ABAQUS, Inc, 1080 Main Street, Pawtucket, RI 02860-4847, 2003.

[15] G. Gazetas and R. Dobry, "Simple radiation damping model for piles and footings", Journal of the Engineering Mechanics Division, ASCE, 110 (6), 931–956, 1984.

[16] G. Gazetas and J.L. Tassoulas, "Horizontal damping of arbitrarily shaped embedded foundations", Journal of Geotechnical Engineering, ASCE, 113, 458–575, 1987.

[17] M. Fotopoulou, P. Kotsanopoulos, G. Gazetas and J.L. Tassoulas, "Rocking damping of arbitrarily shaped embedded foundations", Journal of Geotechnical Engineering, ASCE, 115, 473–490, 1989.

[18] J.P. Wolf and A. Paronesso, "Lumped-parameter model for a rigid cylindrical foundation embedded in a soil layer on rigid rock", Earthquake Engineering and Structural Dynamics, 21, 1021–1038, 1992.

[19] L. Andersen and M. Liingard, "Lumped-parameter models for wind-turbine footings on layered ground". In "Proceedings of the Eleventh International Conference on Civil, Structural and Environmental Engineering Computing", B.H.V. Topping (Editor), Civil-Comp Press, Stirlingshire, Scotland, 2007.